Hindawi Publishing Corporation
International Journal of Chemical Engineering
Volume 2009, Article ID 563420, 7 pages
doi:10.1155/2009/563420

Research Article

Influence of Different Cations of N3 Dyes on Their Photovoltaic Performance and Stability

Luísa Andrade,[1] Shaik M. Zakeeruddin,[2] Mohammad K. Nazeeruddin,[2] Helena Aguilar Ribeiro,[1] Adélio Mendes,[1] and Michael Graetzel[2]

[1] *Laboratory for Process, Environment and Energy Engineering (LEPAE), Department of Chemical Engineering, Faculty of Engineering, University of Porto, 4200-465 Porto, Portugal*
[2] *Laboratory of Photonics and Interfaces, Institute of Chemical Sciences and Engineering, Swiss Federal Institute of Technology, 1015 Lausanne, Switzerland*

Correspondence should be addressed to Shaik M. Zakeeruddin, shaik.zakeer@epfl.ch

Received 16 October 2008; Accepted 13 January 2009

Recommended by Eugénio C. Ferreira

The N3 dye was modified by substituting two of its protons by potassium or sodium cations. The performance and stability of dye-sensitized solar cells incorporating the new dyes were evaluated under light soaking ($1000\,W \cdot m^{-2}$) at 50°C. Photocurrent measurements demonstrated that proton substitution by potassium cations rends the system more stable. Further characterization of the potassium-based devices was performed by electrochemical impedance spectroscopy to investigate the charge-transfer phenomena occurring at the different interfaces of the cells.

1. Introduction

Nowadays, a particular interest in the development of alternative energy sources arises, especially motivated not only by the need of reducing the dependency on fossil fuel resources, but also for providing the reduction of the CO_2 emissions. An attractive strategy to overcome the present energy problem is using renewable energy sources, such as the direct solar radiation, for producing clean energy. In this sense, the direct conversion of sunlight into electricity by means of photovoltaic systems makes an important contribution to this energy contend in an environmentally friendly way [1, 2]. In conventional solar cells, the charge separation occurs at the interface of two materials of different conduction mechanisms, exploiting the photovoltaic effect [3]. More recently, a new generation of cells emerged, the dye-sensitized solar cells (DSCs). DSCs are considered very promising since they use low cost, abundant and environmentally safe raw materials, showing relatively high-energy efficiency [4].

A DSC is made of a nanoparticulated titania film coated with an adsorbed dye monolayer. This thin film is applied on a glass substrate coated with a transparent conducting oxide (TCO) that collects the photoinjected electrons. A back electrode consists of the same conducting glass coated with platinum. This serves as a catalyst for the redox reaction occurring in the electrolyte present in between the two electrodes (Figure 1).

In DSCs, the dye is a crucial component to achieve high overall photoelectric conversion efficiency. Up to now, ruthenium complexes have been widely investigated due to their advantageous spectral properties, device photostability and high conversion efficiency [5–7]. An example of these ruthenium polypyridine complexes with better performance as sensitizer is the cis-di(thiocyanato)bis(4,4′-dicarboxilic acid-2,2′-bipyridine)ruthenium(II), commonly known as N3 [8]. Since the development of the N3 dye in 1993 [8], its tetrabutylammonium (TBA) salt N719 has been used as the standard red dye because of its unmatched performances. Similarly to the N719 dye, new dyes were developed bearing in mind that the number of protons in the dye influences the open-circuit potential and the short circuit current of the DSC [9]. In this work we modified the N3 dye by partially substituting its protons with different cations, namely, sodium and potassium. The modified dyes were subsequently incorporated in final DSC devices, which

were then submitted to accelerated thermal/light soaking aging tests for performance and stability evaluation. The cells were subjected to full sunlight irradiation at 50°C for about 1000 hours, during which time their photovoltaic parameters were periodically monitored.

Electrochemical impedance spectroscopy (EIS) was used to investigate the charge transfer phenomena occurring at the different interfaces of the DSCs. This technique has been widely used for the characterization of several electrochemical systems and, in particular, to analyze internal resistances in the DSCs [10–19]. In 2000 Bisquert et al. applied their models in the analysis of the mechanisms of electron recombination in nanoporous TiO_2 dye-sensitized solar cells [18]. After this first approach, EIS became more and more useful, playing a crucial role in what concerns modeling and understanding the complex charge phenomena occurring in DSCs [10–19]. The charge-transfer resistance at the TCO layer, the charge-transfer resistance at the counter-electrode/electrolyte interface, and the charge-transfer resistance at TiO_2/dye/electrolyte interface can therefore be obtained by fitting the EIS results to appropriate equivalent electrical circuits [20].

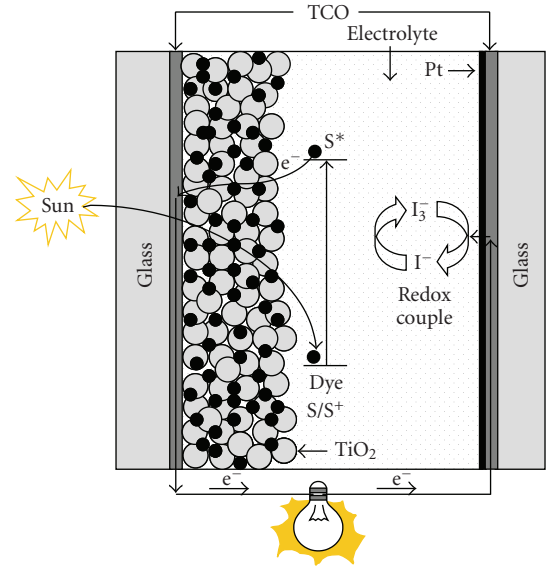

Figure 1: Schematic representation of a dye-sensitized solar cell.

2. Experimental Section

2.1. Dye Preparation. N719 dye was synthesized as reported earlier [21]. The dipotassium [$2K^+$(N3, $2H^+$)] and disodium [$2Na^+$(N3, $2H^+$)] dyes were prepared as follows. First, N719 dye was dissolved in acetonitrile solvent and to this an excess amount of potassium triflate or sodium triflate in acetonitrile was added. Immediately, the triflate counter ion was precipitated, filtered and washed with acetonitrile and dried under vaccum.

2.2. Composition of Electrolyte E1. 0.1 M iodine, 0.5 M N-methylbenzimidazole in a mixture of BMII; PMI TFSI; γ-BL (2; 3; 1) vol/vol.

2.3. TiO_2 *Electrode Preparation.* A screen-printed double layer film of interconnected TiO_2 particles was used as mesoporous negative electrode. A 7-μm thick film of 20-nm-sized TiO_2 particles was first printed on the fluorine-doped SnO_2 conducting glass electrode and further coated by a 5-μm thick second layer of 400-nm-sized light scattering anatase particles. The detailed preparation procedures of TiO_2 nanocrystals, pastes for screen-printing and double-layer nanostructured TiO_2 film have been reported elsewhere [22].

2.4. Dye-Sensitized Solar Cell Fabrication. The working electrode, described above, was sealed to the counter electrode (FTO glass—15 Ω/square—coated with a platinum solution chemically deposited at 450°C for 15 minutes) by means of a 25 μm-thick transparent Surlyn ring (from DuPont) at 130°C for 15 seconds. The cells were filled with an electrolyte solution through a predrilled hole in the counter electrode. The hole was then sealed with a Bynel disc and a thin glass to avoid leakage of the electrolyte.

2.5. Photovoltaic Measurements. All photovoltaic measurements were performed under a 450 W xenon light source able to provide 1000 $W \cdot m^{-2}$ sunlight equivalent irradiation (AM 1.5). The spectral output of the lamp was matched in the region of 350–750 nm with the aid of a Schott K113 Tempax sunlight filter (Präzisions Glas & Optik GmbH, Iserlohn, Germany) so as to reduce the mismatch between the simulated and true solar spectra. Various incident light intensities were regulated with wavelength neutral wire mesh atenuators. *I-V* curves were obtained by applying an external bias to the cells and measuring the respective photocurrent response with a digital source meter (Keithley Instruments Inc., Ohio, USA Model 2400). The incident photon-to-current conversion efficiency (IPCE) was recorded by a data-collecting system as a function of excitation wavelength. The incident light from a 300 W xenon lamp (ILC Technology, Calif, USA) was focused through a Gemini-180 double monochromator (Jobin Yvon., UK) onto the cell under test. The monochromator output was incremented through the visible spectrum to generate the *IPCE* (λ) as defined by $IPCE(\lambda) = 12400(J_{sc}/\lambda\phi)$, where λ is the wavelength (nm), J_{sc} is short-circuit photocurrent density ($mA \cdot cm^{-2}$), and ϕ is the incident radiative flux ($mW \cdot cm^{-2}$). Photovoltaic performance was determined for an active area of 0.158 cm^2 defined by a metal mask.

2.6. Electrochemical Impedance Measurements. Impedance experiments were carried out with a computer-controlled potentiostat (EG&G M273) equipped with a frequency response analyzer (EG&G M1025). The frequency range was 0.005 Hz–100 kHz and the magnitude of the modulation signal was 10 mV. All the measurements were performed at room temperature in the dark at −0.75 V bias. The EIS spectra were fitted to an appropriate electrical analogue by

means of the Z View software (v2.5b, Scribner Associates Inc, NC, USA).

2.7. Stability Tests. Hermetically sealed cells were used to check the long-term stability under visible light soaking at 50°C. The light soaking experiments employed a polymer film of 50-μm thickness (Preservation Equipment Ltd, UK), as a 400 nm UV cut-off filter. Two cells of each type with matched photovoltaic performances were exposed at open circuit to a Suntest CPS lamp (ATLAS Material Testing Solituions, GMBH, 1000 W · m^{-2}, 50°C) over a period of 1000 hours. The cells were taken out at regular intervals to record the photocurrent-voltage curve.

3. Results and Discussion

Figure 2(a) shows the photocurrent density-voltage curves obtained under AM 1.5 simulated sunlight (1000 W · m^{-2}) for DSCs prepared with [2K$^+$(N3, 2H$^+$)], [2Na$^+$(N3, 2H$^+$)], and N719 dyes in association with electrolyte E1. The cells were labelled as device A, B and C, respectively. For simplicity, the results for one single cell of each type are presented hereafter.

Comparing the three systems under study, device C shows the best initial photovoltaic performance. In fact, it is already known by its unmatched performance. On the basis of cations' substitution in the N3 dye, the anchoring groups of the adsorbed sensitizer transfer most of its protons to the semiconductor surface, charging it positively. This change in the TiO_2 surface enhances the adsorption of the anionic ruthenium complexes and favors electron injection from the excited state of the dye into the conduction band of the semiconductor, resulting in higher photocurrents. Nevertheless, this positive shift of the Fermi level induced by surface protonation leads to a low open-circuit potential. In fact, if the sensitizer has less protons, it is expected to obtain high open-circuit potential and low photocurrents, and the other way round if the sensitizer is fully protonated. So, an optimal degree of protonation of the sensitizer should be considered to reach maximum overall conversion efficiency [9]. In this study we observed that the sodium-based system (device B) presents higher values of short-circuit current, J_{sc}, and open-circuit voltage, V_{oc}, than cells with the potassium-based system (device A)—Figure 2(a). However, the latter system has higher overall power conversion efficiency, η, due to a higher value of the fill factor, *FF*. This fact is explained by a reduction in the series resistance of the cell with potassium salt dye.

In Figure 2(b) the incident photon-to-current conversion efficiency (*IPCE*) for devices A, B, and C can be compared. The *IPCE* is plotted as a function of the excitation wavelength. In line with the better photovoltaic performance, device C shows the highest *IPCE*: maximum of about 67% at 530 nm. At the same wavelength, device A reaches a maximum of 54%, while device B reaches approximately 63%.

Apart from efficiency, the long-term stability is also a key issue regarding the industrial development and commercialization of DSCs. Thus, an intimate relation between photovoltaic performances and stability should be achieved. The evolution of the photovoltaic performances throughout the aging process of the three systems under study is presented in Figure 3. Device A reveals a very good stability when compared with the two other systems. Actually, this device kept close to 90% of its initial performance after 1000 hours of light soaking at 50°C. In contrast, devices

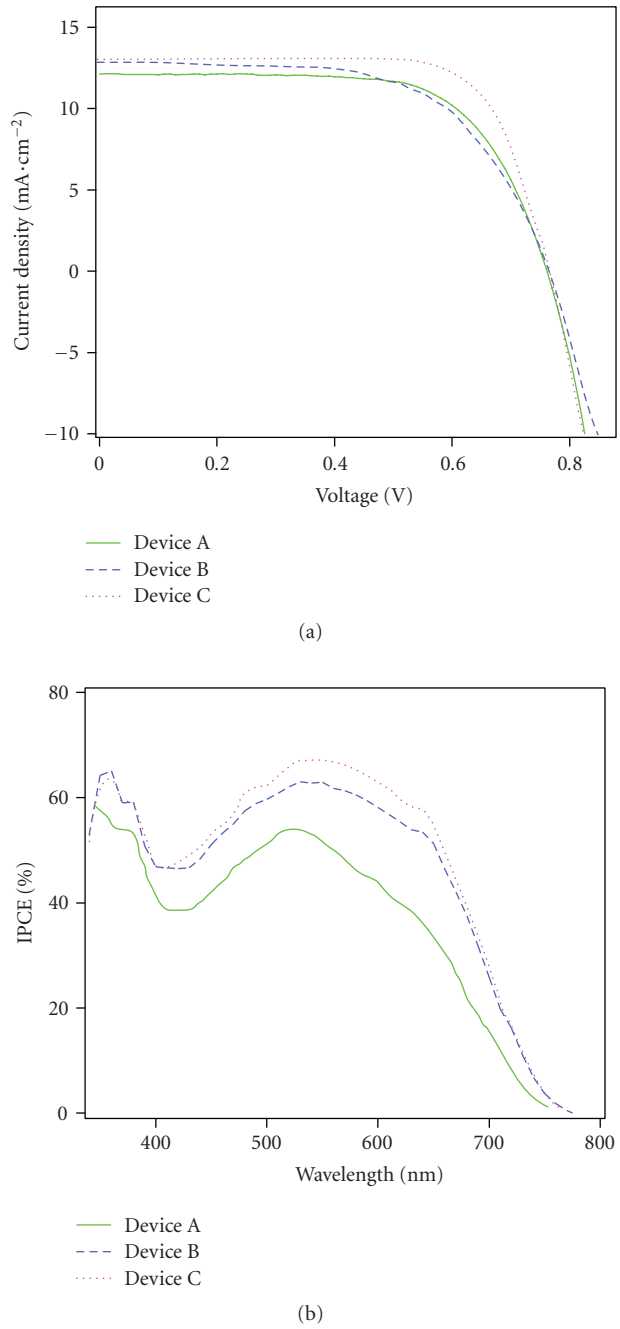

Figure 2: (a) Photocurrent intensity-voltage characteristics for devices A, B, and C, measured at 1 sun (1000 W · m^{-2}), AM 1.5 global sunlight illumination. (b) Photocurrent action spectra of the same devices.

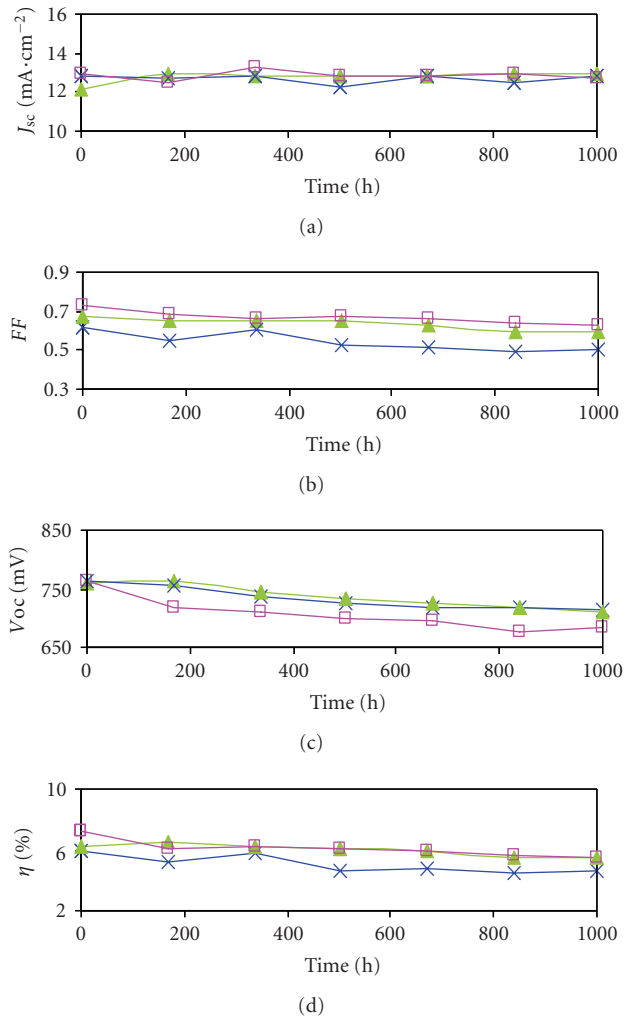

Figure 3: Evolution of photovoltaic parameters for device A (▲), device B (×), and device C (□). The cells were kept under one sun visible-light soaking at 5°C for approximately 1000 hours.

B and C showed a drop in efficiency of about 23% and 25%, respectively. The higher stability of device A is mainly due to an increase in the photocurrent (6%) during the first week of aging, which was then maintained at the same level for the rest of the aging period. Additionally, this system shows a quite stable evolution of the *FF* values, indicating constancy in series resistance during the aging process. Despite its high photovoltaic performance as a fresh cell, the N719 system was unstable, exhibiting a marked decrease in J_{sc} and V_{oc} soon after the first week. This may be due to desorption of dye from the TiO_2 surface. Moreover, the sodium salt containing device B does not rend the system very stable, as suggested by the strong oscillation in all its photovoltaic parameters.

The stability tests allow us to conclude that the number and type of substituting cations will strongly influence the photovoltaic performances of the devices. Considering the ionic potentials of the cations we can realize how strongly they will be electrostatically attracted to ions of opposite charge and to what extent the cations will repel other ions of like-charge. As the sodium cation has higher ionic potential than the potassium cation, we may be induced to say that the stability is improved when substituting the N3 protons by sodium cations. However, this conclusion is not straightforward since we have to considerer the DSC system with all its components. The present work proves this fact since potassium substitution renders a better stability. The positive shift of the Fermi level upon adsorption of the dye decreases the gap between the redox couple and the Fermi level. This fact will strongly influence the TiO_2/dye/electrolyte interaction, which is not totally understood.

Bearing in mind the promising results in terms of performance and long-term stability of the potassium-based DSC, a deeper characterization of the system was performed. In this sense, the effect of the aging process in the overall performance of device A was analyzed by means of electrochemical impedance spectroscopy. This technique allows us to determine the charge-transfer resistances at the platinum counter-electrode and at the TiO_2/dye/electrolyte interface as well as to determine the Nernstian diffusion of I^-/I_3^- ions within the electrolyte [10, 20]. The Bode and Nyquist (Z''-imaginary part of impedance versus Z'-real part of impedance) plots for the potassium-based system, before and after the aging process, are shown in Figure 4.

Several physical models have been developed in an effort to understand all the complex charge-transfer processes that take place in DSCs [15, 18, 23]. These works employ the diffusion-recombination model to study the electronic processes taking place at the semiconductor, whereas the electron transfer phenomena at the electrolyte and contact interfaces are described by simple RC electrical arrangements. Actually, the electron transport and charge recombination in nanocrystalline TiO_2 films have been widely studied by Bisquert et al. [18], who suggested an infinite transmission line model to describe the charge-transfer phenomena occurring at the mesoscopic TiO_2 film, as presented in Figure 5.

The transmission line model assumes the TiO_2 photoanode as an interconnected network where electrons, after excitation, can diffuse toward the external circuit with a resistance R_w or recombine at the TiO_2/electrolyte interface. Assuming that the recombination phenomenon is only related to electron transfer by back reaction with the electrolyte (dark current), it can be described by a charge transfer resistance, R_k, and a chemical capacitance, C_μ. If L is the thickness of the mesoscopic TiO_2 film, the electron transport resistance through the semiconductor is defined as $R_w = r_w L$, while the interfacial charge recombination resistance and the chemical capacitance at the interface are, respectively, $R_k = r_k/L$ and $C_\mu = c_\mu L$.

The other charge-transfer processes occurring in DSCs are also considered in the electrical analogue, as shown in Figure 5. Regeneration of I_3^- at the counter electrode is characterized by R_{CE} and C_{CE}, which represent the charge-transfer resistance and the double-layer capacitance at the platinized FTO glass, respectively.

Finally, the ZView software was used to fit the experimental data to the equivalent circuit presented in Figure 5. For better fitting, all capacitor elements were replaced by

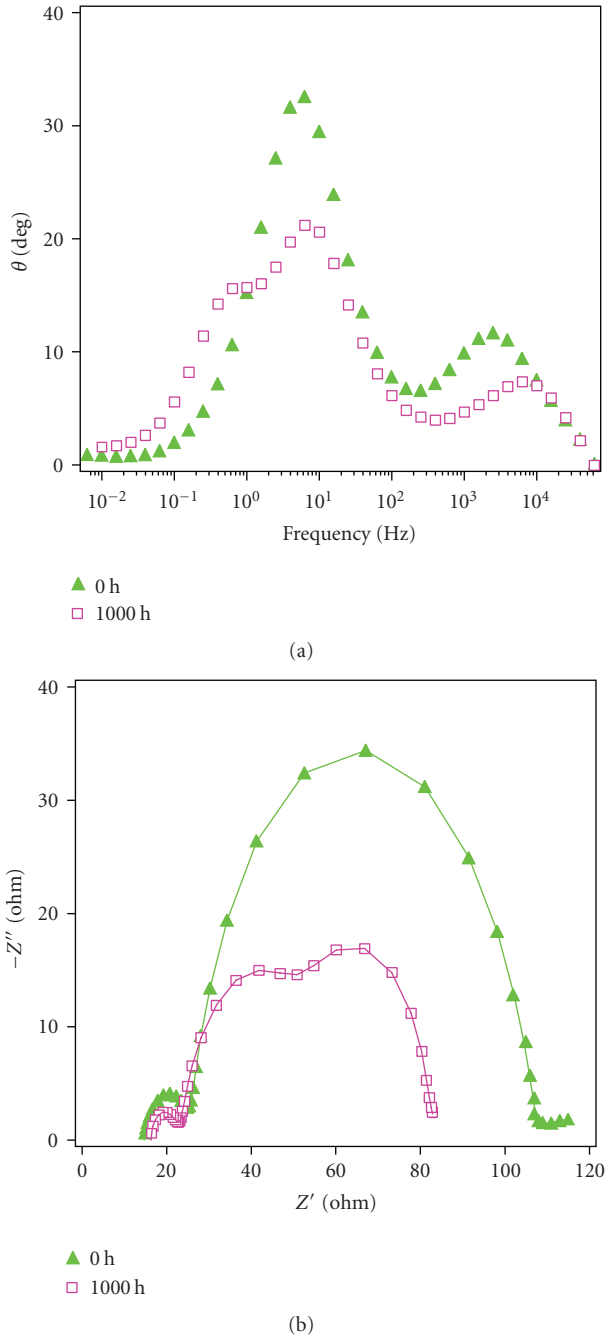

Figure 4: Bode (a) and Nyquist (b) diagrams obtained for device A before and after 1000 hours under thermal/light soaking stress. In the Nyquist diagram, symbols correspond to the impedance data obtained experimentally in the dark under −0.75 V bias, while solid lines represent the fittings according to the equivalent circuit present in Figure 5.

constant phase elements (CPEs), non-ideal capacitances associated with a nonuniform distribution of current in the heterogeneous TiO_2 film [24].

Table 1 presents some parameters useful to understand the underlying mechanisms related to the aging process. Besides R_k and R_w, the electron lifetime τ_n ($\tau_n = R_k C_\mu$),

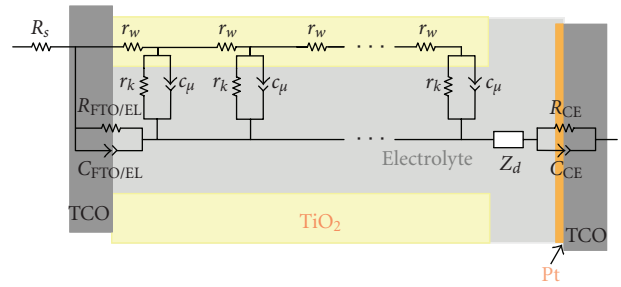

Figure 5: Transmission line model used to fit the EIS experimental data.

the effective electron diffusion length L_n ($L_n = L\sqrt{R_k/R_w}$), and the effective diffusion coefficient of electrons in the TiO_2 semiconductor D_n ($D_n = L_n^2/\tau_n$) can also be obtained [23]. According to the diffusion-recombination model, the ratio R_k/R_w ($\gg 1$) clearly shows that the charge-transfer resistance associated to recombination of electrons at the TiO_2/electrolyte interface (R_k) is much higher than the electron transport resistance through the semiconductor (R_w). This means that the cell exhibits carrier collection efficiency near unity [23].

Moreover, Table 1 shows that L_n is much higher than the thickness of the mesoscopic TiO_2 film ($L \approx 12\,\mu$m) in both fresh and aged cells, confirming the excellent transport properties. The increased J_{sc} for the aged sample can be attributed to the longer electron diffusion length compared to the fresh sample ($J_{sc}^{0\,\text{hours}} = 12.1\,\text{mA}\cdot\text{cm}^{-2}$ and $J_{sc}^{1000\,\text{hours}} = 12.9\,\text{mA}\cdot\text{cm}^{-2}$). As shown in Figure 4(a), the middle frequency peak position of the aged sample was slightly shifted to higher frequencies, revealing a decrease in the electron lifetime. The decreased electron lifetime is mainly ascribed to a major decrease in R_k (in Table 1) for the aged sample compared to the fresh one. This means that electrons recombine more easily with the electrolyte upon aging. A faster electron recapture taking place in the aged device prevents the electron accumulation in the TiO_2 nanoparticles from reaching the same density as for the fresh devices. As a result, the drop of V_{oc} was observed in aged devices (Figure 3). The same conclusions can be drawn from the significant decrease of the intermediate semicircle in Figure 4(b), which corresponds to a lower value of the charge-transfer resistance (R_k) at this interface. The increased electron diffusion coefficient was probably due to the positive shift of the conduction band energy level edge.

A decrease in the redox charge-transfer resistance at the platinum counter electrode was observed upon aging ($R_{CE}^{0\,\text{hours}} = 9.1\,\Omega$ and $R_{CE}^{1000\,\text{hours}} = 5.5\,\Omega$). This explains the decrease of the left-hand side semicircle in the Nyquist diagram. This semicircle corresponds to the high-frequency peak in the Bode plot, which has moved toward larger values (meaning lower electron lifetimes and shorter redox reaction times). Additionally, an overlap between the photoelectrode impedance (middle semicircle) and that related to the Nernstian diffusion within the electrolyte (right-hand semicircle) can be noticed. This was probably due to

Table 1: Parameters determined by fitting the EIS experimental data of device A to the equivalent circuit as shown in Figure 5.

Exposure time/hours	R_k/Ω	R_w/Ω	R_k/R_w	L_n/μm	τ_n/ms	$D_n/\text{cm}^2 \cdot \text{s}^{-1}$
0	67.2	5.1	13.3	25.5	11.1	5.90×10^{-4}
1000	32.3	1.8	18.4	30.0	4.5	2.00×10^{-3}

a larger overpotential for the I^-/I_3^- redox reaction on the platinum electrode of the aged sample, accompanied with a fill factor problem (*FF* decreases from 0.67 to 0.59 upon aging).

4. Conclusion

Two N3-based dyes were synthesized bearing in mind that the number of protons in the sensitizer influences the open-circuit potential and the short circuit current of the DSC. Potassium and sodium cations were used to substitute two protons of the N3 dye and the resulting dyes were compared with the well-known N719 dye that contains two TBA (tetrabutylammonium) cations. Despite presenting the highest initial photovoltaic performance, the N719 system was rather unstable, exhibiting a strong decrease in J_{sc} and V_{oc} upon aging, which might be due to dye desorption. In addition, sodium substitution in place of TBA does not help to enhance the stability of devices, whereas substitution with potassium salt revealed better stability compared to the other two systems. In fact, this system kept close to 90% of its initial performance after 1000 hours of light soaking at 50°C.

Acknowledgments

L. Andrade and H. Aguilar Ribeiro are grateful to the Portuguese Foundation for Science and Techonology (FCT) for their Ph.D and postdoc grants (no. SFRH/BD/30464/2006 and SFRH/BPD/36992/2007, resp.).

References

[1] M. Grätzel, "Molecular photovoltaics that mimic photosynthesis," *Pure and Applied Chemistry*, vol. 73, no. 3, pp. 459–467, 2001.

[2] K. Zweibel, J. Mason, and V. Fthenakis, "By 2050 solar power could end U.S. dependence on foreign oil and slash greenhouse gas emissions," *Scientific American*, vol. 298, no. 1, pp. 64–73, 2008.

[3] M. Grätzel, "Dye-sensitized solar cells," *Journal of Photochemistry and Photobiology C*, vol. 4, no. 2, pp. 145–153, 2003.

[4] M. Grätzel, "Photoelectrochemical cells," *Nature*, vol. 414, no. 6861, pp. 338–344, 2001.

[5] R. Amadelli, R. Argazzi, C. A. Bignozzi, and F. Scandola, "Design of antenna-sensitizer polynuclear complexes. Sensitization of titanium dioxide with $[Ru(bpy)_2(CN)_2]_2 Ru(bpy(COO)_2)_2^{2-}$," *Journal of the American Chemical Society*, vol. 112, no. 20, pp. 7099–7103, 1990.

[6] R. Argazzi, C. A. Bignozzi, T. A. Heimer, F. N. Castellano, and G. J. Meyer, "Enhanced spectral sensitivity from ruthenium(II) polypyridyl based photovoltaic devices," *Inorganic Chemistry*, vol. 33, no. 25, pp. 5741–5749, 1994.

[7] S. Ruile, O. Kohle, P. Péchy, and M. Grätzel, "Novel sensitisers for photovoltaic cells. Structural variations of Ru(II) complexes containing 2,6-bis(1-methylbenzimidazol-2-yl)pyridine," *Inorganica Chimica Acta*, vol. 261, no. 2, pp. 129–140, 1997.

[8] M. K. Nazeeruddin, A. Kay, I. Rodicio, et al., "Conversion of light to electricity by *cis*-X_2bis(2,2′-bipyridyl-4,4′-dicarboxylate)ruthenium(II) charge-transfer sensitizers (X = Cl^-, Br^-, I^-, CN^-, and SCN^-) on nanocrystalline titanium dioxide electrodes," *Journal of the American Chemical Society*, vol. 115, no. 14, pp. 6382–6390, 1993.

[9] M. K. Nazeeruddin, R. Humphry-Baker, P. Liska, and M. Grätzel, "Investigation of sensitizer adsorption and the influence of protons on current and voltage of a dye-sensitized nanocrystalline TiO_2 solar cell," *The Journal of Physical Chemistry B*, vol. 107, no. 34, pp. 8981–8987, 2003.

[10] R. Kern, R. Sastrawan, J. Ferber, R. Stangl, and J. Luther, "Modeling and interpretation of electrical impedance spectra of dye solar cells operated under open-circuit conditions," *Electrochimica Acta*, vol. 47, no. 26, pp. 4213–4225, 2002.

[11] A. N. M. Green, E. Palomares, S. A. Haque, J. M. Kroon, and J. R. Durrant, "Charge transport versus recombination in dye-sensitized solar cells employing nanocrystalline TiO_2 and SnO_2 films," *The Journal of Physical Chemistry B*, vol. 109, no. 25, pp. 12525–12533, 2005.

[12] L. Han, N. Koide, Y. Chiba, and T. Mitate, "Modeling of an equivalent circuit for dye-sensitized solar cells," *Applied Physics Letters*, vol. 84, no. 13, pp. 2433–2435, 2004.

[13] L. Han, N. Koide, Y. Chiba, et al., "Improvement of efficiency of dye-sensitized solar cells by reduction of internal resistance," *Applied Physics Letters*, vol. 86, no. 21, Article ID 213501, 3 pages, 2005.

[14] J. Bisquert, "Theory of the impedance of electron diffusion and recombination in a thin layer," *The Journal of Physical Chemistry B*, vol. 106, no. 2, pp. 325–333, 2002.

[15] M. Adachi, M. Sakamoto, J. Jiu, Y. Ogata, and S. Isoda, "Determination of parameters of electron transport in dye-sensitized solar cells using electrochemical impedance spectroscopy," *The Journal of Physical Chemistry B*, vol. 110, no. 28, pp. 13872–13880, 2006.

[16] F. Fabregat-Santiago, J. Bisquert, G. Garcia-Belmonte, G. Boschloo, and A. Hagfeldt, "Influence of electrolyte in transport and recombination in dye-sensitized solar cells studied by impedance spectroscopy," *Solar Energy Materials and Solar Cells*, vol. 87, no. 1–4, pp. 117–131, 2005.

[17] F. Fabregat-Santiago, G. Garcia-Belmonte, J. Bisquert, A. Zaban, and P. Salvador, "Decoupling of transport, charge storage, and interfacial charge transfer in the nanocrystalline TiO_2/electrolyte system by impedance methods," *The Journal of Physical Chemistry B*, vol. 106, no. 2, pp. 334–339, 2002.

[18] J. Bisquert, G. Garcia-Belmonte, F. Fabregat-Santiago, N. S. Ferriols, P. Bogdanoff, and E. C. Pereira, "Doubling exponent models for the analysis of porous film electrodes by impedance. Relaxation of TiO_2 nanoporous in aqueous solution," *The Journal of Physical Chemistry B*, vol. 104, no. 10, pp. 2287–2298, 2000.

[19] J. Bisquert, A. Zaban, and P. Salvador, "Analysis of the mechanisms of electron recombination in nanoporous TiO_2 dye-sensitized solar cells. Nonequilibrium steady-state statistics and interfacial electron transfer via surface states," *The Journal of Physical Chemistry B*, vol. 106, no. 34, pp. 8774–8782, 2002.

[20] F. Fabregat-Santiago, J. Bisquert, E. Palomares, et al., "Correlation between photovoltaic performance and impedance spectroscopy of dye-sensitized solar cells based on ionic liquids," *The Journal of Physical Chemistry C*, vol. 111, no. 17, pp. 6550–6560, 2007.

[21] M. K. Nazeeruddin, S. M. Zakeeruddin, R. Humphry-Baker, et al., "Acid-base equilibria of (2,2′-bipyridyl-4,4′-dicarboxylic acid)ruthenium(II) complexes and the effect of protonation on charge-transfer sensitization of nanocrystalline titania," *Inorganic Chemistry*, vol. 38, no. 26, pp. 6298–6305, 1999.

[22] D. Kuang, S. Ito, B. Wenger, et al., "High molar extinction coefficient heteroleptic ruthenium complexes for thin film dye-sensitized solar cells," *Journal of the American Chemical Society*, vol. 128, no. 12, pp. 4146–4154, 2006.

[23] Q. Wang, S. Ito, M. Grätzel, et al., "Characteristics of high efficiency dye-sensitized solar cells," *The Journal of Physical Chemistry B*, vol. 110, no. 50, pp. 25210–25221, 2006.

[24] J. R. Macdonal, *Impedance Spectroscopy*, John Wiley & Sons, New York, NY, USA, 2005.